Vapor-liquid equilibria of ethylene (C_2H_4) + decafluorobutane (C_4F_{10}) at 268 to 298 K from experiment, molecular simulation and the Peng-Robinson equation of state

Andreas Köster[1], Prabir Nandi[2], Thorsten Windmann[1], Deresh Ramjugernath[2], Jadran Vrabec[1] *

[1] Lehrstuhl für Thermodynamik und Energietechnik, Universität Paderborn, Warburger Straße 100, 33098 Paderborn, Germany

[2] Thermodynamics Research Unit, School of Engineering, University of KwaZulu Natal, Durban 4041, South Africa

Keywords: Vapor-liquid equilibrium; Decafluorobutane; Ethylene; Experiment; Molecular simulation; Peng-Robinson equation of state

Abstract

Isothermal vapor-liquid equilibrium (VLE) data are presented for the system ethylene + decafluorobutane. Measurements are performed for four isotherms around the critical temperature of ethylene, i.e. in the temperature range from 268.13 to 298.13 K. The measurements are undertaken using a "static-analytic" type apparatus, sampling the phases in equilibrium via a moving capillary sampler (ROLSI^{TM}). The uncertainties of the present measurements of temperature, pressure and mole fraction are within 0.036 K, 0.0058 MPa and 0.02 mol/mol, respectively. The VLE data are correlated with the Peng-Robinson equation of state (PR EOS), incorporating the Mathias-Copeman alpha function. Both, the Wong-Sandler (WS) mixing rule with the non-random two-liquid (NRTL) activity coefficient model and the quadratic Van der Waals one-fluid mixing rule are used. In addition, a new rigid force field model for decafluorobutane is developed and molecular simulations are carried out. The simulation results are compared to the present experimental data for the binary system. Furthermore, pure component properties of decafluorobutane are predicted and compared to experimental data from the literature and the PR EOS.

* corresponding author, tel.: +49-5251/60-2421, fax: +49-5251/60-3522, email: jadran.vrabec@upb.de

1 Introduction

In preceding work, vapor-liquid equilibrium (VLE) data of binary systems containing decafluorobutane (C_4F_{10}) and ethane [1] as well as CO_2 [2] were presented. The scope of this work is to extend the current understanding of perfluorocarbons (PFC) as physical solvents by studying VLE data of the binary system ethylene (C_2H_4) + C_4F_{10} by experiment, molecular simulation and the Peng-Robinson equation of state (PR EOS). The interest in PFC stems from their large capacity to dissolve gases [1–3] so that the potential of PFC as physical solvents in petrochemical refinery gas absorption processes should be explored.

Our literature review revealed that the binary system C_2H_4 + C_4F_{10} has not been studied prior to this work. Experimental VLE data of this system will thus help to improve the parameters of EOS or group contribution methods to describe or predict the thermophysical properties and the phase equilibrium behavior of multi-component systems containing such binary pairs. Binary VLE data were measured here with a "static-analytic" apparatus that was equipped with a rapid online sampler injector (ROLSI^{TM}) [4] and a gas chromatograph (GC) for equilibrium vapor and liquid phase sample handling and analysis. The experimental data were correlated with the direct method in THERMOPACK [5] with the PR EOS [6], incorporating the Mathias-Copeman [7] alpha function, using either the Wong-Sandler (WS) [8] mixing rule with the non-random two-liquid (NRTL) [9] activity coefficient model or the quadratic Van der Waals one-fluid mixing rule [10].

To carry out molecular simulations of the present system, a new force field model for C_4F_{10} was developed. The parameterization of the molecular model was carried out on the basis of the quantum chemical (QC) calculations, followed by optimizations to experimental data on vapor pressure and saturated liquid density. Molecular simulation data for pure C_4F_{10} as well as for the mixture C_2H_4 + C_4F_{10} are presented and compared to experimental data from the literature and from this work. The simulation results for pure C_4F_{10} are only reported graphically, the numerical values are given in the Supplementary Material.

2 Experimental

2.1 Materials

Decafluorobutane (C_4F_{10}, CAS number: 355-25-9) was supplied by Pelchem (South Africa) with a certified purity greater than 98 vol-%. Ethylene (C_2H_4, CAS number: 74-85-1) was purchased from Air Products (South Africa) with a certified purity greater than 99.9 vol-%. Both chemicals were used in their purchased form because their GC analysis did not exhibit the presence of significant impurities. The critical properties and the acentric factor [11] of these two compounds are listed in Table 1.

2.2 Experimental Apparatus and Procedure

The apparatus that was used here to measure VLE data is based on a "static-analytic" method with an accurate sampling of the two coexisting (vapor and liquid) phases via a mobile ROLSI^{TM} sampler [12], a sampling technique developed by the Centre for Energy and Processes of the Thermodynamics and Phase Equilibria group (CEP/TEP) at MINES ParisTech, Fontainebleau, France. This equipment was documented in detail elsewhere [13,14]. In short, the equilibrium cell with an internal volume of 17.4 (± 0.22) cm^3, which is the main part of the apparatus, consists of a cylindrical sapphire tube held between two stainless steel flanges. The apparatus was designed and constructed to operate between 253 and 473 K for absolute pressures below 20 MPa. The equilibrium cell was fully immersed in a liquid bath for temperature regulation.

The temperature of the equilibrium cell was measured with two platinum resistance thermometers (Pt-100) that are inserted into the top and the bottom flange of the equilibrium cell. The two Pt-100 probes were initially calibrated against a standard Pt-100 probe using a processor calibrator (type CPH6000, WIKA). The standard probe was certified to have an accuracy of ± 0.03 K.

The pressure was measured with a pressure transducer (type P10, WIKA) with an accuracy of 0.05 % in the range from 0 to 10 MPa. This sensor was calibrated against a standard pressure transducer (type CPT 6000, WIKA) with an accuracy of 0.025 %. Pressure and temperature data were recorded via a computer that was linked to a data acquisition unit (type 34970A, Agilent). The resulting combined uncertainties

of the temperature and pressure measurements were estimated to be ± 0.036 K and ± 0.0058 MPa, respectively.

The analysis of samples of the equilibrium phases was performed with a GC (type GC-2010, Shimadzu) that was equipped with a thermal conductivity detector (TCD). The analytical column (Q type, Porapak) had a 80/100 mesh (1/8" Silcosteel tube, 4 m length). The TCD was calibrated using the direct method, since the components were gaseous and standard binary solutions could not be prepared. Taking into account the uncertainties due to calibration and analysis, the resulting uncertainties for the present vapor and liquid mole fractions were estimated to be less than ± 0.02 mol/mol.

The experimental procedure was similar to the one that was described by Coquelet et al. [15]. Prior to any measurements, the equilibrium cell and its associated loading lines were evacuated at room temperature to a pressure of approximately 0.1 Pa. The cell was then loaded with C_2H_4, the more volatile component, and allowed to reach the specified equilibrium temperature of the measurement. Equilibrium was assumed when the two Pt-100 probes gave the same temperature values within their uncertainty for at least 10 minutes. After recording the vapor pressure of C_2H_4 at the specified temperature, the cell was evacuated and C_4F_{10} was loaded into the cell. C_2H_4 was then added to the cell such that successive equilibrium mixtures with a gradually increasing overall gaseous content were prepared. Each addition of C_2H_4 to the equilibrium cell was followed by a measurement of the temperature T, pressure p, vapor mole fraction y and liquid mole fraction x on the two phase envelope. Throughout, equilibrium was assumed when the total pressure reading remained constant within the measuring uncertainty over a period of 10 minutes of stirring. For every equilibrium state point, at least five samples of both the vapor and the liquid phase were taken with the ROLSI^{TM} sampler and analyzed to check for the reproducibility of the measurements.

3 Theory and Modelling

3.1 Equation of State

The present experimental VLE data were correlated using the non-commercial proprietary software THERMOPACK, developed by CEP/TEP at MINES ParisTech [5]. This was done with the well known PR EOS

[10]

$$p = \frac{RT}{v-b} - \frac{a(T)}{v\cdot(v+b)+b\cdot(v-b)}, \tag{1}$$

where

$$a(T) = 0.45724\frac{(RT_c)^2}{p_c}\alpha(T), \tag{2}$$

and

$$b = 0.07780\frac{RT_c}{p_c}. \tag{3}$$

Therein, v is the molar volume, R is the ideal gas constant, T_c is the critical temperature and p_c is the critical pressure.

For an accurate representation of the vapor pressure of the two components, the Mathias-Copeman [7] alpha function

$$\alpha(T) = \left[1 + c_1\cdot\left(1-\sqrt{\frac{T}{T_c}}\right) + c_2\cdot\left(1-\sqrt{\frac{T}{T_c}}\right)^2 + c_3\cdot\left(1-\sqrt{\frac{T}{T_c}}\right)^3\right]^2, \tag{4}$$

for $T < T_c$, and

$$\alpha(T) = \left[1 + c_1\cdot\left(1-\sqrt{\frac{T}{T_c}}\right)\right]^2, \tag{5}$$

for $T > T_c$, was used. Therein, c_1, c_2 and c_3 are adjustable parameters. All pure fluid parameters were taken from the literature [1,16] and are listed in Table 1.

To represent the present binary VLE data, two different mixing rules were considered in the PR EOS. First, the WS mixing rule [8], based on the NRTL [9] activity coefficient model with the adjustable parameters $k_{i,j}$, $\tau_{i,j}$ and $\tau_{j,i}$, was taken. The temperature-dependent parameters $\tau_{i,j}$ and $\tau_{j,i}$ were adjusted directly to the present VLE data by means of a modified simplex algorithm minimizing the objective function

$$f = \frac{100}{N}\left[\sum\left(\frac{x_{EOS}-x_{exp}}{x_{exp}}\right)^2 + \sum\left(\frac{y_{EOS}-y_{exp}}{y_{exp}}\right)^2\right]. \tag{6}$$

Therein, N is the number of data points, x_{EOS} and x_{exp} are the calculated and measured liquid phase mole fractions and y_{EOS} and y_{exp} are the corresponding vapor phase mole fractions, respectively.

Second, the quadratic Van der Waals one-fluid mixing rule [10] was chosen. It is a much simpler model with a single temperature-independent binary parameter $k_{i,j}$ that was also adjusted to the present VLE

data.

Generally, temperature-independent binary interaction parameters are preferred to enhance the applicability of EOS beyond the temperature range that was considered in the adjustment. Here, this approach led to significant deviations as discussed below. In order to reach a more precise representation of the data and simultaneously minimize the objective function, two sets of binary interaction parameters for the WS mixing rule were used: one for the isotherms below the critical temperature of C_2H_4 and another one for the isotherms above the critical temperature of C_2H_4.

3.2 Pure Component Molecular Modelling

To develop a rigid, non-polarizable molecular model, three types of parameters have to be taken into account. These are (1) the geometric parameters, specifying the positions of different interaction sites, (2) the electrostatic parameters, defining the polar interactions in terms of point charges, dipoles or quadrupoles, and (3) the dispersive and repulsive parameters, determining the attraction by London forces and the repulsion by electronic orbital overlaps. In the present work, the Lennard-Jones (LJ) 12-6 potential was used to describe the dispersive and repulsive interactions. In this case, the total intermolecular interaction energy writes as

$$
\begin{aligned}
U = \sum_{i=1}^{N-1} \sum_{j=i+1}^{N} \Bigg\{ & \sum_{a=1}^{S_i^{LJ}} \sum_{b=1}^{S_j^{LJ}} 4\varepsilon_{ijab} \left[\left(\frac{\sigma_{ijab}}{r_{ijab}} \right)^{12} - \left(\frac{\sigma_{ijab}}{r_{ijab}} \right)^{6} \right] + \\
& \sum_{c=1}^{S_i^e} \sum_{d=1}^{S_j^e} \frac{1}{4\pi\varepsilon_0} \left[\frac{q_{ic} q_{jd}}{r_{ijcd}} + \frac{q_{ic}\mu_{jd} + \mu_{ic} q_{jd}}{r_{ijcd}^2} \cdot f_1\left(\boldsymbol{\omega}_i, \boldsymbol{\omega}_j\right) + \frac{q_{ic} Q_{jd} + Q_{ic} q_{jd}}{r_{ijcd}^3} \cdot f_2\left(\boldsymbol{\omega}_i, \boldsymbol{\omega}_j\right) + \right. \\
& \left. \frac{\mu_{ic}\mu_{jd}}{r_{ijcd}^3} \cdot f_3\left(\boldsymbol{\omega}_i, \boldsymbol{\omega}_j\right) + \frac{\mu_{ic} Q_{jd} + Q_{ic}\mu_{jd}}{r_{ijcd}^4} \cdot f_4\left(\boldsymbol{\omega}_i, \boldsymbol{\omega}_j\right) + \frac{Q_{ic} Q_{jd}}{r_{ijcd}^5} \cdot f_5\left(\boldsymbol{\omega}_i, \boldsymbol{\omega}_j\right) \right] \Bigg\}, \qquad (7)
\end{aligned}
$$

where r_{ijab}, ε_{ijab} and σ_{ijab} are the distance, the LJ energy parameter and the LJ size parameter, respectively, for the pair-wise interaction between LJ site a on molecule i and LJ site b on molecule j. The permittivity of the vacuum is ε_0, whereas q_{ic}, μ_{ic} and Q_{ic} denote the point charge magnitude, the dipole moment and the quadrupole moment of the electrostatic interaction site c on molecule i and so forth. The expressions $f_x(\boldsymbol{\omega}_i, \boldsymbol{\omega}_j)$ stand for the dependence of the electrostatic interactions on the orientations $\boldsymbol{\omega}_i$ and $\boldsymbol{\omega}_j$ of the

molecules i and j, cf. [17,18]. Finally, the summation limits N, S_x^{LJ} and S_x^e denote the number of molecules, the number of LJ sites and the number of electrostatic sites, respectively.

Despite its large size, the C_4F_{10} molecule was modeled without its internal degrees of freedom, cf. Figure 1. In contrast to other approaches [2,19], the present force field was thus chosen to be rigid. This choice was primarily driven by the current limitations of the molecular simulation tool $ms2$ [20] that was employed in this work.

Using the software package GAMESS(US), QC calculations were carried out to obtain the geometric structure of the molecule in its energetically most favorable state. Therefore, the Hartree-Fock level of theory was applied with a relatively small (6-31G) basis set. Each atom of the molecule was represented by one LJ site and one point charge so that the model consists of 14 LJ sites and 14 point charges. The LJ parameters ε and σ were initially taken from a model for 1,1,1,2,3,3,3-heptafluoropropane (R227ea) [21]. A Mulliken population analysis [22] was performed to obtain the point charge magnitudes q. To optimize the molecular model, saturated liquid density and vapor pressure were fitted to experimental data [23–25] by varying the LJ parameters. Subsequently, all model parameters were fine-tuned using the reduced unit method [26]. In comparison to the R227ea model, the LJ parameters ε and σ were altered by -0.8 % and -0.3 % for the carbon atoms and by +7.1 % and +2.2 % for the fluorine atoms, respectively. All parameters of the present molecular model are given in Table 2.

For C_2H_4, a molecular model from previous work was taken [27]. It is a two-center LJ model with a pointquadrupole (2CLJQ) that describes the VLE with an accuracy of about 0.5 % for the saturated liquid density, 3-4 % for the vapor pressure and 2-3 % for the enthalpy of vaporization over the whole temperature range from the triple point to the critical point [27].

3.3 Molecular Modelling of Mixtures

To describe mixtures on the basis of pairwise additive potentials, molecular modeling reduces to the specification of the interaction between unlike molecules. The unlike polar interactions were treated in a physically straightforward manner without using binary parameters. For the unlike LJ interactions, the

modified Lorentz-Berthelot combination rule with one state-independent binary parameter was used [28]

$$\sigma_{ijab} = \frac{\sigma_{iiaa} + \sigma_{jjbb}}{2}, \tag{8}$$

and

$$\varepsilon_{ijab} = \xi \sqrt{\varepsilon_{iiaa} \cdot \varepsilon_{jjbb}}. \tag{9}$$

The binary parameter ξ was adjusted to a single experimental data point, i.e. vapor pressure of the mixture. An equimolar liquid mole fraction is most recommended for the adjustment to the vapor pressure, because the binary parameter has the strongest influence under these conditions. For the present system, the vapor pressure $p = 3.3176$ MPa at $T = 298.13$ K and $x_{\mathrm{C2H4}} = 0.48$ mol/mol, which was measured in this work, was used to adjust it to $\xi = 0.87$.

3.4 Molecular Simulation Details

In this work, the Grand Equilibrium method [29] was used for the VLE calculations of both C_4F_{10} and C_2H_4 + C_4F_{10}. To determine the chemical potential of pure C_4F_{10} in the liquid, gradual insertion [30,31] was used for temperatures $T \leq 225$ K, while for higher temperatures, Widom's test molecule method [32] was applied. For gradual insertion, MC simulations in the NpT ensemble were performed using 864 molecules. Starting from a face-centered cubic lattice, 30,000 MC cycles were sampled for equilibration with the first 10,000 time steps in the canonical (NVT) ensemble. The production run was performed for 120,000 steps. For Widom's test molecule method, MD simulations using 864 molecules were performed. Again starting from a face-centered cubic lattice, 30,000 time steps were sampled for equilibration with the first 10,000 time steps in the canonical (NVT) ensemble. The production run was performed for 150,000 steps. The time step was set to 2.0 fs, the integrator used in this study was the Gear-predictor corrector. The chemical potential using Widom's test molecule method was determined by inserting 3,456 virtual molecules into the simulation volume and averaging over all results. For the corresponding vapor, the simulation volume was adjusted to lead to an average number of 500 molecules. After 10,000 initial NVT MC cycles, starting from a face centered cubic lattice, 15,000 equilibration cycles in the pseudo-μVT ensemble were performed. The length of the production run was 150,000 cycles.

For the mixture $C_2H_4 + C_4F_{10}$ the chemical potential in the liquid was throughout calculated with Widom's test molecule method [32]. The same settings as described above were used for both the liquid and the vapor simulations. Thermodynamic properties were determined in the production phase of the simulation on the fly. The statistical uncertainties of all results were estimated by block averaging according to Flyvbjerg and Petersen [33] and the error propagation law.

4 Results and Discussion

4.1 Modelling Results for Decafluorobutane

The molecular C_4F_{10} model and the PR EOS were evaluated by comparison to experimental data [23–25,34–36] and to correlations thereof [37] from the literature. In case of the VLE behavior, correlations from the DIPPR database, with a stated error of <3 % for the saturated liquid density, <5 % for the vapor pressure and <10 % for the enthalpy of vaporization, were used [37]. Furthermore, the second virial coefficient was compared to a correlation from the DIPPR database with a stated error of <5 % and an average absolute uncertainty of ±0.76 l/mol [37]. All present pure C_4F_{10} simulation data are available in numerical form in the Supplementary Material.

Figure 2 presents the saturated densities in absolute terms. The deviation plot in Figure 3 allows for a more detailed inspection of the saturated liquid density. Compared to both the DIPPR correlation [37] and the experimental data [23,24], the molecular model yields very satisfactory results throughout the entire temperature range from 190 to 358 K. An absolute mean deviation of 0.6 % between the molecular simulation data and the DIPPR correlation was achieved, which is well within the uncertainty of the correlation. With an absolute mean deviation of 4.0 %, the agreement of the PR EOS to the DIPPR correlation for the saturated liquid density is significantly worse. Vapor pressure data are shown in Figures 3 and 4. For this property, the achieved agreement from both molecular simulation and the PR EOS is good. By inspection of the deviation plot in Figure 3, it can be seen that the statistical scatter of the simulation data is significant at low temperatures. This is underlined by the large statistical simulation uncertainties. Absolute mean deviations of 5.9 % for the molecular simulation data and 2.0 % for the present PR EOS from the DIPPR correlation were obtained. The very large statistical uncertainty of the vapor pressure

from molecular simulation at 250 K is due to the use of the Widom method [32] for the calculation of the chemical potential, which is not suitable for dense and strongly interacting liquids. At 190, 210 and 225 K, the gradual insertion method [30,31] was used instead, resulting in smaller uncertainties of the VLE properties. Figures 3 and 5 show the enthalpy of vaporization. Especially at lower temperatures, the enthalpy of vaporization was overestimated by the molecular model. The PR EOS underestimates this property. The mean deviations to the DIPPR correlation are 5.1 % for the molecular model and 1.5 % for the PR EOS, respectively.

Finally, Figure 6 presents the molecular simulation results in comparison to experimental data [34–36] and to the DIPPR correlation [37] for the second virial coefficient. The achieved agreement is very satisfying. The average absolute deviation is only 0.08 l/mol, which is well within the uncertainty of the DIPPR correlation.

4.2 Binary VLE Measurements and Modelling

The full set of the present experimental VLE data along with the standard deviations for liquid and vapor mole fractions are listed in Table 3. The correlated VLE data are graphically presented together with the experimental and simulated data in Figure 7.

The two sets of NRTL parameters for the WS mixing rule are linearly temperature dependent. For the isotherms below the critical temperature of C_2H_4

$$\tau_{\mathrm{C2H4,C4F10}} = 64.07\frac{\mathrm{J}}{\mathrm{mol}\cdot\mathrm{K}}\cdot T - 9187\frac{\mathrm{J}}{\mathrm{mol}}, \tag{10}$$

and

$$\tau_{\mathrm{C4F10,C2H4}} = 11012\frac{\mathrm{J}}{\mathrm{mol}} - 39.136\frac{\mathrm{J}}{\mathrm{mol}\cdot\mathrm{K}}\cdot T, \tag{11}$$

were used. Isotherms above the critical temperature of C_2H_4 were modelled with

$$\tau_{\mathrm{C2H4,C4F10}} = 14.089\frac{\mathrm{J}}{\mathrm{mol}\cdot\mathrm{K}}\cdot T - 2251.5\frac{\mathrm{J}}{\mathrm{mol}}, \tag{12}$$

and

$$\tau_{\mathrm{C4F10,C2H4}} = 20259\frac{\mathrm{J}}{\mathrm{mol}} - 62.895\frac{\mathrm{J}}{\mathrm{mol}\cdot\mathrm{K}}\cdot T. \tag{13}$$

At the same time, two different temperature-independent values $k_{\mathrm{C2H4,C4F10}} = 0.3714$ for $T < T_{c,\mathrm{C2H4}}$ and $k_{\mathrm{C2H4,C4F10}} = 0.5005$ for $T > T_{c,\mathrm{C2H4}}$ were used. The discontinuity at the critical temperature of C_2H_4 of the correlated model parameters is shown in Figure 8. A similar trend was also observed earlier [38–41]. In total, ten binary parameters (five for $T < T_{c,\mathrm{C2H4}}$ and five for $T > T_{c,\mathrm{C2H4}}$) were used for this PR EOS model.

For the quadratic Van der Waals one-fluid mixing rule only one temperature-independent binary parameter $k_{\mathrm{C2H4,C4F10}}$ was adjusted to the same experimental data point that was used for the adjustment of the binary interaction parameter ξ of the molecular model, i.e. $k_{\mathrm{C2H4,C4F10}} = 0.147$.

Two quantitative measures for fit quality, Bias and average absolute deviation (AAD) of the liquid and vapor mole fractions, are defined by

$$\mathrm{Bias} = \frac{1}{N} \sum \left(\frac{x_{EOS} - x_{exp}}{x_{exp}} \right), \tag{14}$$

and

$$\mathrm{AAD} = \frac{1}{N} \sum \left| \frac{x_{EOS} - x_{exp}}{x_{exp}} \right|, \tag{15}$$

where N represents the number of VLE data points.

These indicators, as listed in Table 5, were used to quantify the agreement between the two parameterizations of the PR EOS and the molecular model with respect to the experimental data. Bias may exhibit either positive or negative values, however, the better the fit of the data, the closer it is to zero. The AAD, by definition, can only be positive and is a better indicator of the fit quality. It can be seen in Table 5 that the experimental data are better represented by the the PR EOS with the WS mixing rule. Bias is mainly below ± 1 % and the AAD is well below 2 %. For the PR EOS with the quadratic mixing rule, these values are mainly around 1.5 % and below 4 %, respectively. Furthermore, the agreement between both versions of the PR EOS and the experimental data is better on the saturated vapor line than on the saturated liquid line. At 288.16 K and lower pressures, the PR EOS with the WS mixing rule is higher than the experimental data, cf. Figure 7. In addition, the saturated vapor line at 268.13 K and lower pressures is slightly underestimated by this version of the PR EOS. Apart from that, the agreement can be considered as excellent. The course of the PR EOS with the quadratic mixing rule is a little different.

At lower pressures, this version of the PR EOS is throughout below the version with the WS mixing rule.

Another option to present VLE data is the relative volatility

$$\alpha_{\mathrm{C2H4,C4F10}} = \frac{y_{\mathrm{C2H4}}/x_{\mathrm{C2H4}}}{y_{\mathrm{C4F10}}/x_{\mathrm{C4F10}}}, \tag{16}$$

which can be seen in Figure 9. Especially at higher mole fractions x_{C2H4}, the relative volatility from experiment and the WS mixing rule PR EOS were found to be in good agreement. At lower mole fractions x_{C2H4}, the PR EOS with the quadratic mixing rule exhibits a different slope which better matches with the experimental data. The agreement of this property from molecular simulation is not as good, especially for lower temperatures. In addition, the molecular simulation data exhibit a quite large scatter for this property.

Bias and AAD values of the molecular simulation data in comparison with the PR EOS with the WS mixing rule are shown in Table 5. For the saturated liquid line, these indicators are mainly between ± 5 and 10 %. The agreement on the saturated vapor line is better. Here, Bias and AAD are well below ± 4 %. It can be seen from the uniformly negative Bias values that the molecular simulation data exhibit too high mole fractions x_{C2H4} and y_{C2H4} throughout the entire temperature range. Only at higher pressures, the x_{C2H4} values from simulation are smaller than those modelled with the PR EOS and the WS mixing rule, cf. Figure 7. Overall, the molecular simulation data agree reasonably with both the experimental data and the two versions of PR EOS.

5 Conclusion

New high pressure phase equilibrium data were measured for the binary system ethylene + decafluorobutane at temperatures from 268.13 to 298.13 K using an apparatus based on the "static-analytic" method. The measured data were correlated with the PR EOS, incorporating the Mathias-Copeman alpha function. In case of the binary VLE data, both the Wong-Sandler mixing rule with the NRTL activity coefficient model and the quadratic Van der Waals one-fluid mixing rule were used. The uncertainties of the present measurements were ± 0.036 K, ± 0.0058 MPa and ± 0.02 mol/mol for temperature, pressure and mole fractions, respectively. Molecular simulations were carried out and compared to the experimental data and

the PR EOS. For this purpose, a new molecular model for decafluorobutane was developed. Molecular simulations for pure decafluorobutane and the binary mixture ethylene + decafluorobutane lead to reasonable results, although the C_4F_{10} molecule was modelled without internal degrees of freedom.

Acknowledgements

This work was partially based upon research supported by the South African Research Chairs Initiative of the Department of Science and Technology and National Research Foundation. The authors gratefully acknowledge financial support by Bundesministerium für Bildung und Forschung, BMBF-Projekt SUA 09/020. The simulations were performed on the national super computer NEC Nehalem Cluster "laki" at the High Performance Computing Center Stuttgart (HLRS) and on the HP X6000 super computer at the Steinbuch Centre for Computing, Karlsruhe. Prabir Nandi is grateful to the University of Kwa-Zulu Natal for providing a post doctoral fellowship. Furthermore, Andreas Köster would like to thank the Ernest-Solvay Foundation for granting a scholarship that made this work possible.

List of Symbols

Abbreviations

AAD	average absolute deviation
CEP/TEP	Centre for Energy and Processes of the Thermodynamics and Phase Equilibria Group
EOS	equation of state
GC	gas chromatograph
LJ	Lennard-Jones
NRTL	non-random two-liquid
PFC	Perfluorocarbon
PR	Peng-Robinson
Pt-100	platinum resistance thermometer, basic resistance 100 Ω
QC	quantum chemical
TCD	thermal conductivity detector
VLE	vapor-liquid equilibria
WS	Wong-Sandler

Latin Letters

a	attractive parameter of the Peng-Robinson equation of state
b	volume parameter of the Peng-Robinson equation of state
B	second virial coeficient
c_i	adjustable parameters of the Mathias-Copeman alpha function
Δh_v	enthalpy of vaporization
k_B	Boltzmann constant
k_{ij}	binary parameter of the Peng-Robinson equation of state
N	number of data points
N	number of molecules
p	pressure
q	point charge magnitude
Q	quadrupole moment magnitude
r	distance

S	number of Lennard-Jones or electrostatic sites
R	ideal gas constant
T	temperature
U	total intermolecular interaction energy
v	molar volume
x	mole fraction in liquid phase
y	mole fraction in vapor phase
x	coordinate with respect to the x axis
y	coordinate with respect to the y axis
z	coordinate with respect to the z axis

Greek Letters

α	Mathias-Copeman alpha function
α	relative volatility
ε	Lennard-Jones energy parameter
ε_0	permittivity of the vacuum
μ	dipolar moment magnitude
ξ	binary interaction parameter
ρ	density
σ	Lennard-Jones size parameter
τ	adjustable parameter of the present Peng-Robinson equation of state
ω	acentric factor
$\boldsymbol{\omega}_x$	orientation of molecule x

Subscripts

a	related to Lennard-Jones site a
ab	related to Lennard-Jones sites a and b
b	related to Lennard-Jones site b
c	related to the critical state
c	related to electrostatic interaction site c
d	related to electrostatic interaction site d

EOS	related to an equation of state
exp	related to an experimental measurement d
i	related to component i
ij	related to components i and j
j	related to component j

Superscripts

LJ	related to Lennard-Jones sites
e	related to electrostatic sites

References

[1] E.E. Ahmar, A. Valtz, P. Naidoo, C. Coquelet, D. Ramjugernath, J. Chem. Eng. Data 56 (2011) 1918-1924.

[2] A. Valtz, X. Courtial, E. Johansson, C. Coquelet, D. Ramjugernath, Fluid Phase Equilib. 304 (2011) 44-51.

[3] J.G. Riess, Chem. Rev. 101 (2001) 2797-2920.

[4] P. Guilbot, A. Valtz, H. Legendre, D. Richon, Analysis 28 (2000) 426-431.

[5] C. Coquelet, A. Baba-Ahmed, 2002, THERMOPACK, version 1.10, Ecole des Mines de Paris, Laboratory of Thermodynamics and Phase Equilibria, Paris, France.

[6] D.Y. Peng, D.B. Robinson, Ind. Eng. Chem. Fundam. 15 (1976) 59-64.

[7] P.M. Mathias, T.W. Copeman, Fluid Phase Equilib. 13 (1983) 91-108.

[8] D.S.H. Wong, S.I. Sandler, AIChE J. 38 (1992) 671-680.

[9] H. Renon, J.M. Prausnitz, AIChE J. 14 (1968) 135-144.

[10] J.M. Smith, H.C. Van Ness, M.M. Abbott, Introduction to chemical engineering thermodynamics, 5th ed. McGraw-Hill, New York, 1996.

[11] Dortmund Data Bank (DDB) version 2011, DDBST Software and Separation Technology GmbH, Oldenburg, Germany.

[12] C. Coquelet, A. Chareton, A. Valtz, A. Baba-Ahmed, D. Richon, J. Chem. Eng. Data 48 (2003) 317-323.

[13] C. Narasigadu, Design of a Static Micro-Cell for Phase Equilibrium Measurements: Measurements and Modelling, Ph.D. thesis, University of Kwa-Zulu Natal, Durban, South Africa, 2011.

[14] C. Narasigadu, P. Naidoo, C. Coquelet, D. Richon, D. Ramjugernath, A novel Static Analytical Apparatus for Phase Equilibrium Measurement, submitted to Fluid Phase Equilib., 2012.

[15] C. Coquelet, D.N. Hong, A. Chareton, A. Baba-Ahmed, D. Richon, Int. J. Refrig. 26 (2003) 559-565.

[16] Aspen Plus, 2008, Version V7.0, Aspen Technology Inc., Burlington, MA, United States.

[17] M.P. Allen, D.J. Tildesley, Computer simulations of liquids, Oxford University Press, Oxford, 1987.

[18] C.G. Gray, K.E. Gubbins, Theory of molecular fluids. 1. Fundamentals, Clarendon Press, Oxford, 1984.

[19] L. Zhang, J.I. Siepmann, J. Phys. Chem. B 109 (2005) 2911-2919.

[20] S. Deublein, B. Eckl, J. Stoll, S.V. Lishchuk, G. Guevara-Carrion, C.W. Glass, T. Merker, M. Bernreuther, H. Hasse, J. Vrabec, Comp. Phys. Commun. 182 (2011) 2350-2367.

[21] B. Eckl, Y.-L. Huang, J. Vrabec, H. Hasse, Fluid Phase Equilib. 260 (2007) 177-182.

[22] R.S. Mulliken, J. Chem. Phys. 36 (1964) 3428-3440.

[23] J.A. Brown, W.H. Mears, J. Phys. Chem. 62 (1958) 960-962.

[24] R.D. Fowler, J.M. Hamilton Jr., J.S. Kasper, C. Weber, W.B. Burford III, H.C. Anderson, Ind. Eng. Chem. 39 (1947) 375-378.

[25] J.W. Mausteller, Ph.D. thesis, Pennsylvania State College, 1951.

[26] J. Stoll, Molecular Models for the Prediction of Thermalphysical Properties of Pure Fluids and Mixtures. Fortschritt-Berichte VDI, Reihe 3, Vol. 836, VDI-Verlag, Düsseldorf, 2005.

[27] J. Vrabec, J. Stoll, H. Hasse, J. Phys. Chem. B 105 (2001) 12126-12133.

[28] T. Schnabel, J. Vrabec, H. Hasse, J. Mol. Liq. 135 (2007) 170-178.

[29] J. Vrabec and H. Hasse, Mol. Phys. 100 (2002) 3375-3383.

[30] I. Nezbeda, J. Kolafa, Mol. Sim. 5 (1991) 391-403.

[31] J. Vrabec, M. Kettler, H. Hasse, Chem. Phys. Lett. 356 (2002) 431-436.

[32] B. Widom, J. Chem. Phys. 39 (1963) 2808-2812

[33] H. Flyvbjerg and H.G. Petersen, J. Chem. Phys. 91 (1989) 461-466.

[34] T.B. Tripp, R.D. Dunlap, J. Phys. Chem. 66 (1962) 635-639.

[35] W. Brostow, D.M. McEachern, S. Perez-Gutierrez, J. Chem. Phys. 71 (1979) 2716-2722.

[36] D.W. McCann, A Group Contribution Method for Second Virial Coefficients, M.Sc. thesis, Pennsylvania State University, 1982.

[37] R.L. Rowley, W.V. Wilding, J.L. Oscarson, Y. Yang, N.A. Zundel, T.E. Daubert, R.P. Danner, DIPPR Information and Data Evaluation Manager for the Design Institute for Physical Properties, AIChE, New York, Version 5.0.2, 2011.

[38] A. Valtz, C. Coquelet, A. Baba-Ahmed, D. Richon, Fluid Phase Equilib. 207 (2003) 53-67.

[39] A. Chapoy, C. Coquelet, D. Richon, Fluid Phase Equilib. 214 (2003) 101-117.

[40] A. Valtz, C. Coquelet, D. Richon, Fluid Phase Equilib. 220 (2004) 77-83.

[41] D. Ramjugernath, A. Valtz, C. Coquelet, D. Richon, J. Chem. Eng. Data 54 (2009) 1292-1296.

Table 1
Sample data, critical properties and acentric factor [11] as well as Mathias-Copeman coefficients for ethylene (C_2H_4) [16] and decafluorobutane (C_4F_{10}) [1] taken from the literature.

Component	C_2H_4	C_4F_{10}
Source	Air Products (South Africa)	Pelchem (South Africa)
Initial purity/vol-%	99.9	98.0
Purification method	none	none
T_c/K	282.35	385.84
p_c/MPa	5.042	2.290
ω	0.085	0.372
c_1	0.50753	0.93487
c_2	-0.04897	-0.48485
c_3	0.30992	2.09290

Table 2
Parameters of the new molecular model for decafluorobutane developed in this work. Lennard-Jones interaction sites and point charge magnitudes are denoted by the modeled atom. Coordinates are given with respect to the center of mass in a principal axes system.

Interaction site	x	y	z	σ	ε/k_B	q
	Å	Å	Å	Å	K	e
C1	-1.6822	0.2798	-0.9876	2.8020	10.5549	0.8774
C2	-0.1821	0.0740	-0.7473	2.8020	10.5549	0.4975
C3	0.2340	0.1133	0.7276	2.8020	10.5549	0.4975
C4	1.6400	-0.4323	1.0036	2.8020	10.5549	0.8774
F1	-2.3735	-0.7873	-0.5805	2.8884	58.6998	-0.2648
F2	-0.6419	-0.6210	1.4543	2.8884	58.6998	-0.2871
F3	0.1571	-1.1281	-1.2709	2.8884	58.6998	-0.2871
F4	1.6681	-1.7578	0.8472	2.8884	58.6998	-0.2648
F5	-1.8919	0.4583	-2.2953	2.8884	58.6998	-0.2700
F6	-2.1085	1.3612	-0.3243	2.8884	58.6998	-0.2697
F7	1.9808	-0.1374	2.2616	2.8884	58.6998	-0.2700
F8	0.1968	1.3969	1.1467	2.8884	58.6998	-0.2833
F9	0.4816	1.0506	-1.4033	2.8884	58.6998	-0.2833
F10	2.5217	0.1296	0.1680	2.8884	58.6998	-0.2697

Table 3
Pressure p, liquid mole fraction x_{C2H4} and vapor mole fraction y_{C2H4} for the binary mixture C_2H_4 + C_4F_{10} at 268.13, 278.36, 288.16 and 298.13 K from present experiments. The number in parentheses indicates the standard deviation of the composition measurement in the last digit(s).[a]

p/MPa	x_{C2H4}/mol mol^{-1}	y_{C2H4}/mol mol^{-1}	p/MPa	x_{C2H4}/mol mol^{-1}	y_{C2H4}/mol mol^{-1}
$T = 268.13$ K			$T = 278.36$ K		
0.0910[b]	0	0	0.1346[b]	0	0
0.4340[c]	0.066	0.744	0.4181[c]	0.049	0.636
0.7635	0.127	0.848	0.7646	0.105	0.794
1.1148	0.194	0.888	1.1393	0.164	0.857
1.4808	0.283	0.911	1.4144	0.216	0.881
1.7910	0.371	0.926	1.7325	0.284	0.900
2.0789	0.463	0.931	2.0261	0.351	0.911
2.3778	0.575	0.941	2.3222	0.427	0.910
2.5953	0.666	0.947	2.6167	0.511	0.920
2.8595	0.775	0.955	2.8628	0.586	0.927
3.0621	0.851	0.957	3.1796	0.685	0.927
3.2471	0.908	0.967	3.4594	0.771	0.935
3.4556	0.952	0.981	3.6551	0.826	0.941
3.6485[b]	1	1	4.0772	0.919	0.957
			4.6112[b]	1	1
$T = 288.16$ K			$T = 298.13$ K		
0.1929[b]	0	0	0.2688[b]	0	0
0.4854[c]	0.045	0.589	0.5709[c]	0.044	0.503
0.9047[c]	0.110	0.739	1.0514[c]	0.110	0.706
1.3008[c]	0.169	0.807	1.5575	0.174	0.793
1.6431	0.222	0.847	2.1568	0.268	0.829
1.9996	0.286	0.871	2.5110	0.329	0.852
2.3165	0.351	0.886	2.9026	0.401	0.872
2.5739	0.406	0.896	3.3176	0.483	0.887
2.7643	0.449	0.901	3.7034	0.564	0.888
2.9772	0.499	0.907	4.0834	0.614	0.896
3.3245	0.586	0.916	4.4999	0.698	0.904
3.6676	0.672	0.921	4.9314	0.781	0.913
3.9442	0.739	0.927	5.1152	0.823	0.916
4.8745	0.916	0.937			

[a] u(T) = 0.036 K, u(p) = 0.0058 MPa, and u(x_{C2H4}) = u(y_{C2H4}) = 0.02 mol mol^{-1}

[b] vapor pressure of pure component

[c] not included into the fit of the PR EOS with the Wong-Sandler mixing rule

Table 4
Pressure p, liquid mole fraction x_{C2H4} and vapor mole fraction y_{C2H4} for the binary mixture C_2H_4 + C_4F_{10} from present molecular simulations.[a]

p/MPa	x_{C2H4}/mol mol^{-1}	y_{C2H4}/mol mol^{-1}	p/MPa	x_{C2H4}/mol mol^{-1}	y_{C2H4}/mol mol^{-1}
T = 268.13 K			T = 278.36 K		
0.09 (2)	0	0	0.13 (1)	0	0
0.34 (2)	0.05	0.71 (3)	0.38 (2)	0.05	0.70 (4)
0.80 (1)	0.15	0.89 (1)	0.92 (1)	0.15	0.86 (1)
1.67 (1)	0.35	0.935 (4)	1.94 (2)	0.35	0.92 (1)
2.11 (2)	0.50	0.955 (4)	2.55 (2)	0.50	0.937 (3)
2.55 (2)	0.65	0.965 (2)	3.13 (2)	0.65	0.950 (2)
2.85 (2)	0.75	0.972 (2)	3.43 (2)	0.75	0.959 (2)
T = 288.16 K			T = 298.13 K		
0.18 (1)	0	0	0.27 (1)	0	0
0.49 (1)	0.05	0.59 (2)	0.61 (2)	0.05	0.51 (1)
1.10 (1)	0.15	0.81 (1)	1.28 (2)	0.15	0.75 (1)
2.16 (2)	0.35	0.90 (1)	2.52 (2)	0.35	0.872 (3)
2.98 (2)	0.50	0.921 (2)	3.40 (2)	0.50	0.895 (3)
3.63 (2)	0.65	0.932 (2)	4.25 (2)	0.65	0.908 (2)
4.03 (2)	0.75	0.943 (1)	4.61 (2)	0.75	0.928 (2)

[a] The number in parentheses indicates the statistical uncertainty in the last digit.

Table 5
Relative deviation Bias and AAD for the two versions of the PR EOS compared to the experimental data and for the molecular simulation data compared to the PR EOS with the Wong-Sandler mixing rule for the binary system C_2H_4 + C_4F_{10}.

	PR EOS with Wong-Sandler mixing rule			
T / K	Bias x %	AAD x %	Bias y %	AAD y %
268.13 K	-1.6	1.6	0.4	0.5
278.36 K	0.8	1.3	-0.1	0.3
288.16 K	-1.4	1.7	0.2	0.3
298.13 K	1.0	1.4	-0.1	0.3
	PR EOS with quadratic mixing rule			
T / K	Bias x %	AAD x %	Bias y %	AAD y %
268.13 K	0.2	3.8	1.2	1.2
278.36 K	1.6	3.8	0.8	0.8
288.16 K	2.3	3.9	0.2	0.8
298.13 K	2.5	4.0	-1.6	1.9
	molecular simulation			
T / K	Bias x %	AAD x %	Bias y %	AAD y %
268.13 K	-7.4	8.4	-1.2	1.7
278.36 K	-5.2	7.1	-3.7	3.7
288.16 K	-10.8	10.8	-1.6	1.6
298.13 K	-5.4	5.8	-0.3	1.9

List of Figures

Fig. 1. Present molecular force field model for decafluorobutane. The green spheres represent the fluorine atoms, the (hardly visible) black spheres represent the carbon atoms. Note that the sphere diameters correspond to the Lennard-Jones size parameters, which are depicted according the molecular geometry scale.

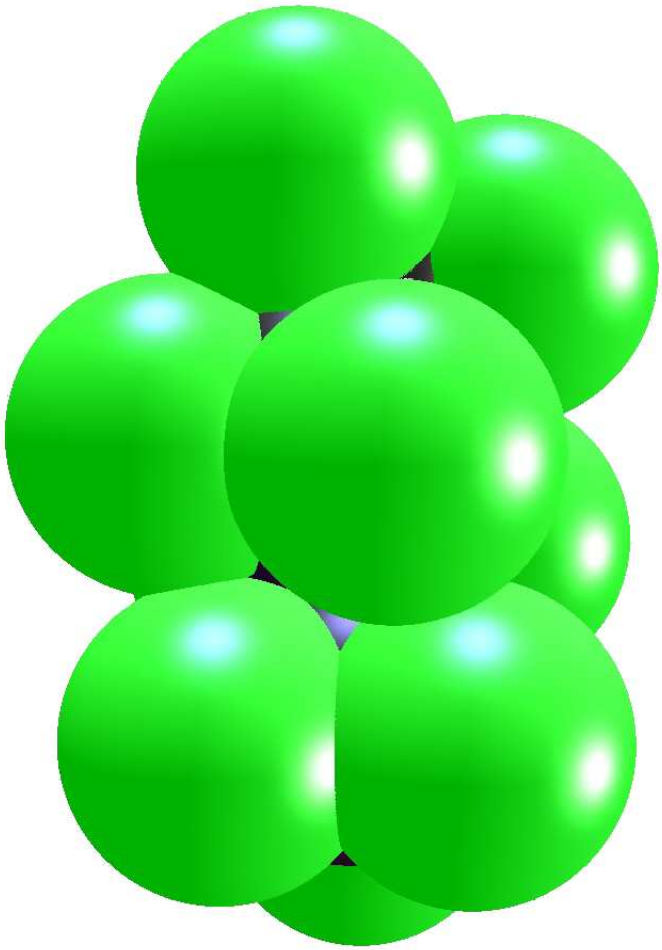

Fig. 2. Saturated densities of perfluorobutane: ○ simulation results, this work, △ critical point of the present molecular model, + experimental data [23,24], - - - DIPPR correlation of experimental data [37], — PR EOS. The statistical uncertainties of the simulation data are within symbol size.

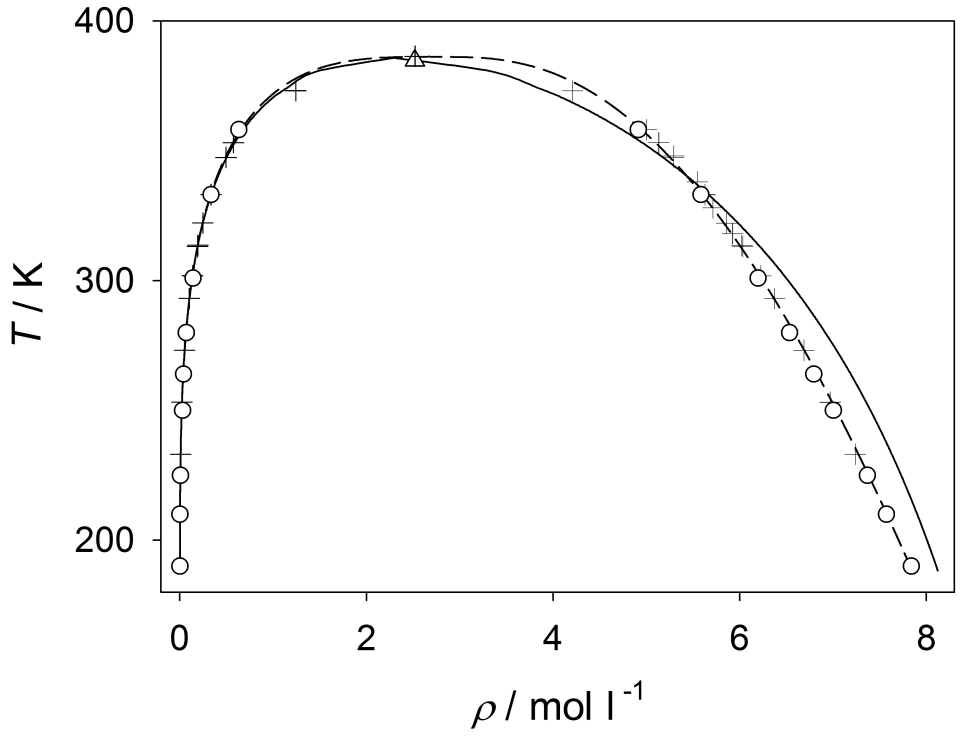

Fig. 3. Relative deviations of vapor-liquid equilibrium properties of decafluorobutane. Simulation data, experimental data [23–25] and the PR EOS are compared to the DIPPR correlation [37] ($\delta z = (z_i - z_{\mathrm{DIPPR}})/z_{\mathrm{DIPPR}}$): ∘ simulation data, this work, + experimental data, — PR EOS. Top: vapor pressure, center: saturated liquid density, bottom: enthalpy of vaporization. The statistical uncertainties of the molecular simulation data are not shown if they are within symbol size.

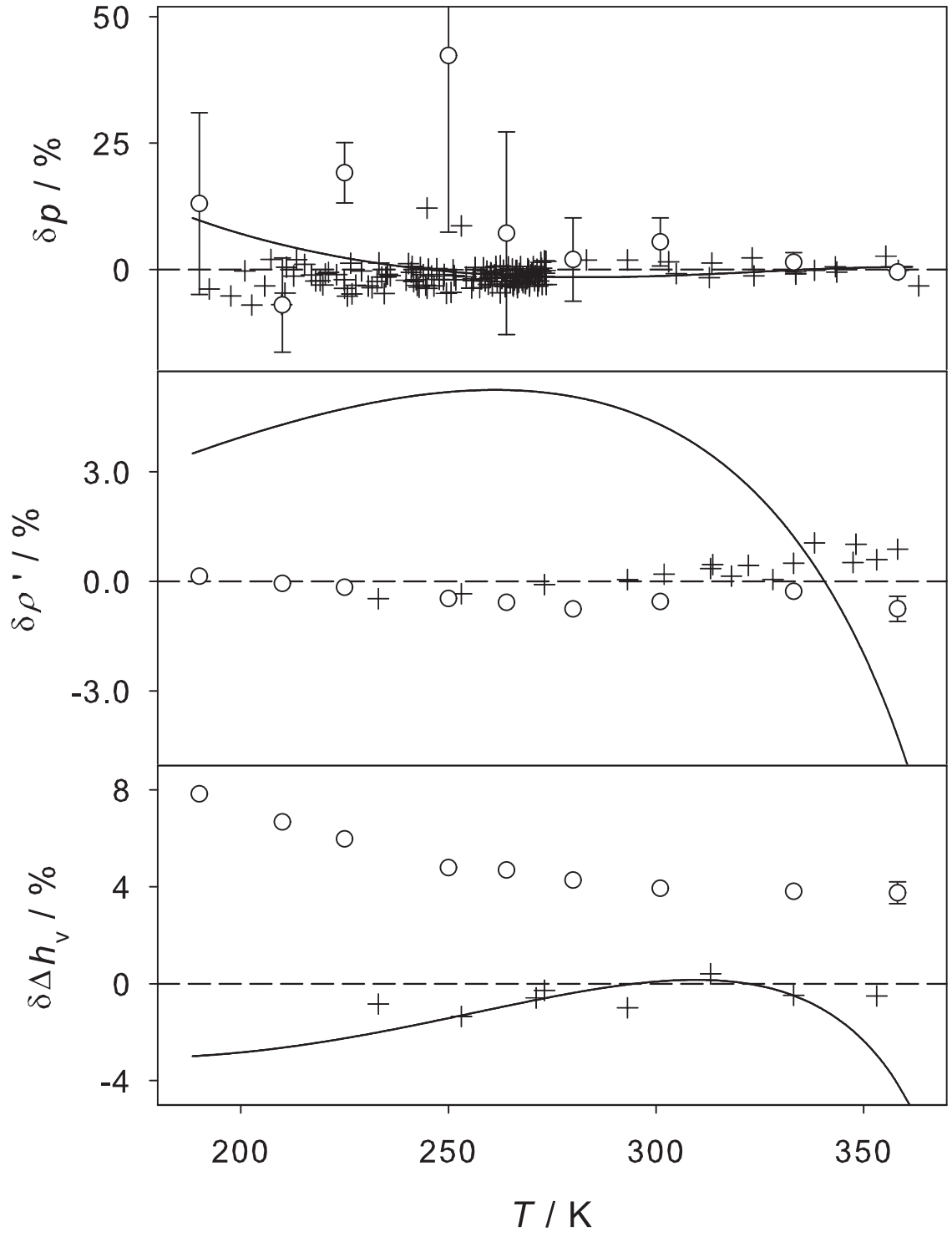

Fig. 4. Vapor pressure of perfluorobutane: ∘ simulation results, this work, △ critical point of the present molecular model, + experimental data [23–25], - - - DIPPR correlation of experimental data [37] (hardly visible), — PR EOS. The statistical uncertainties of the simulation data are within symbol size.

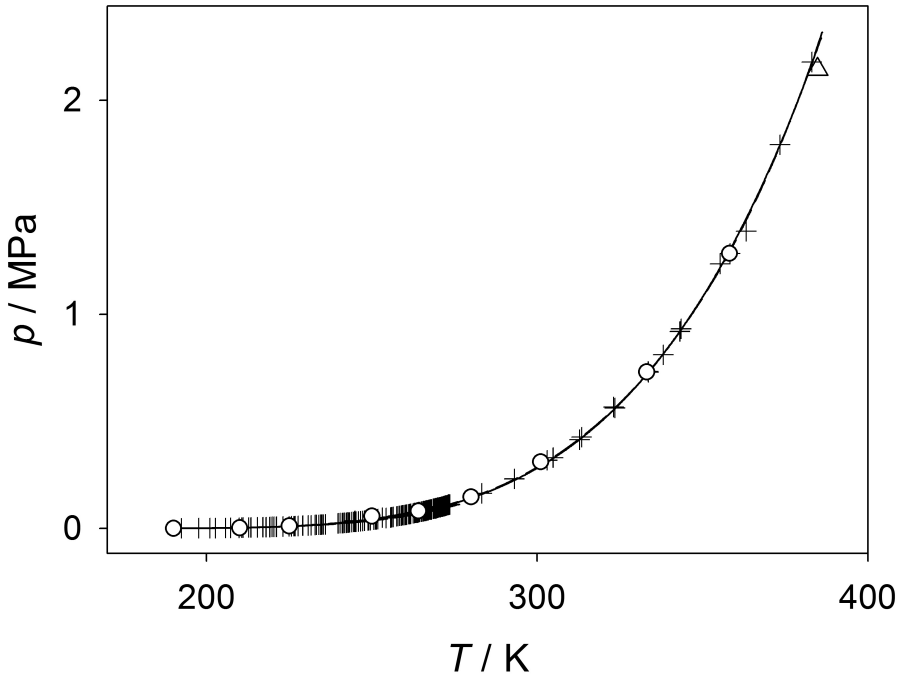

Fig. 5. Enthalpy of vaporization of perfluorobutane: ∘ simulation results, this work, + experimental data [23], - - - DIPPR correlation of experimental data [37], — PR EOS. The statistical uncertainties of the simulation data are within symbol size.

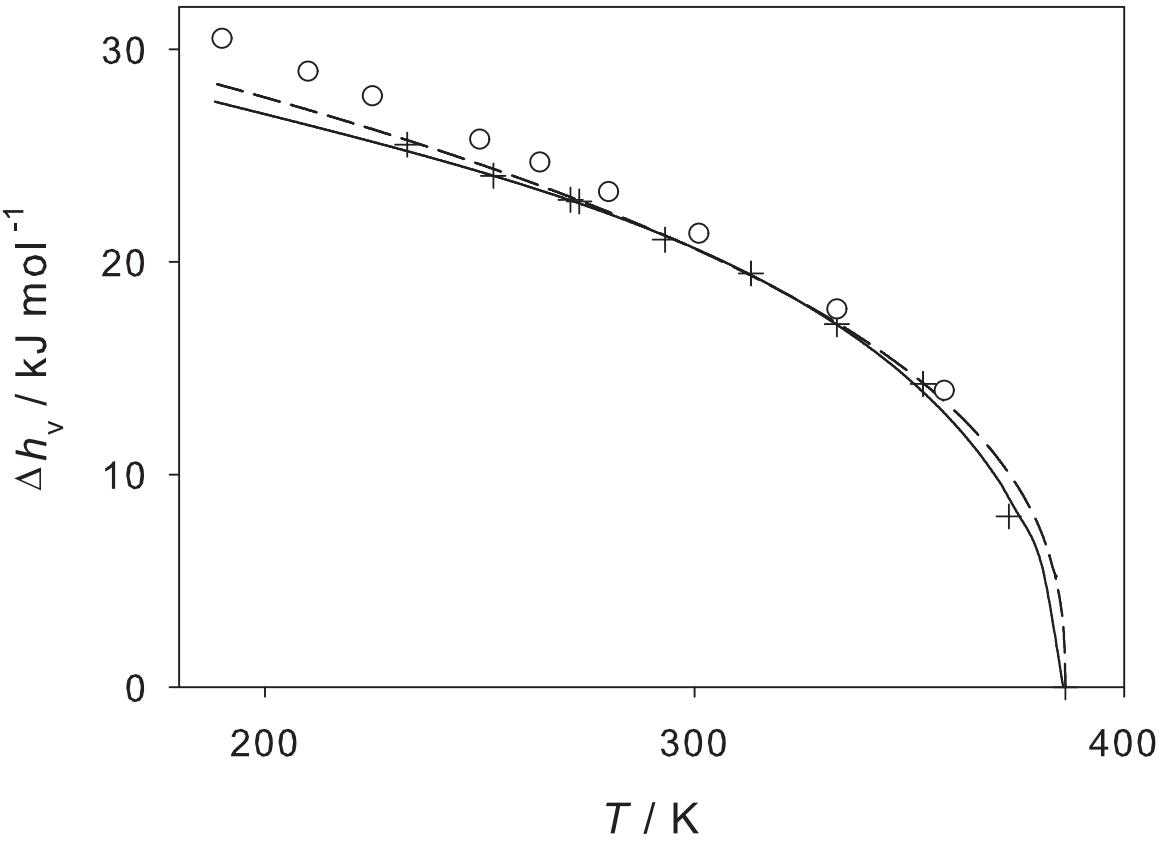

Fig. 6. Second virial coefficient of perfluorobutane: ∘ simulation results, this work, + experimental data [34–36], - - - DIPPR correlation of experimental data [37].

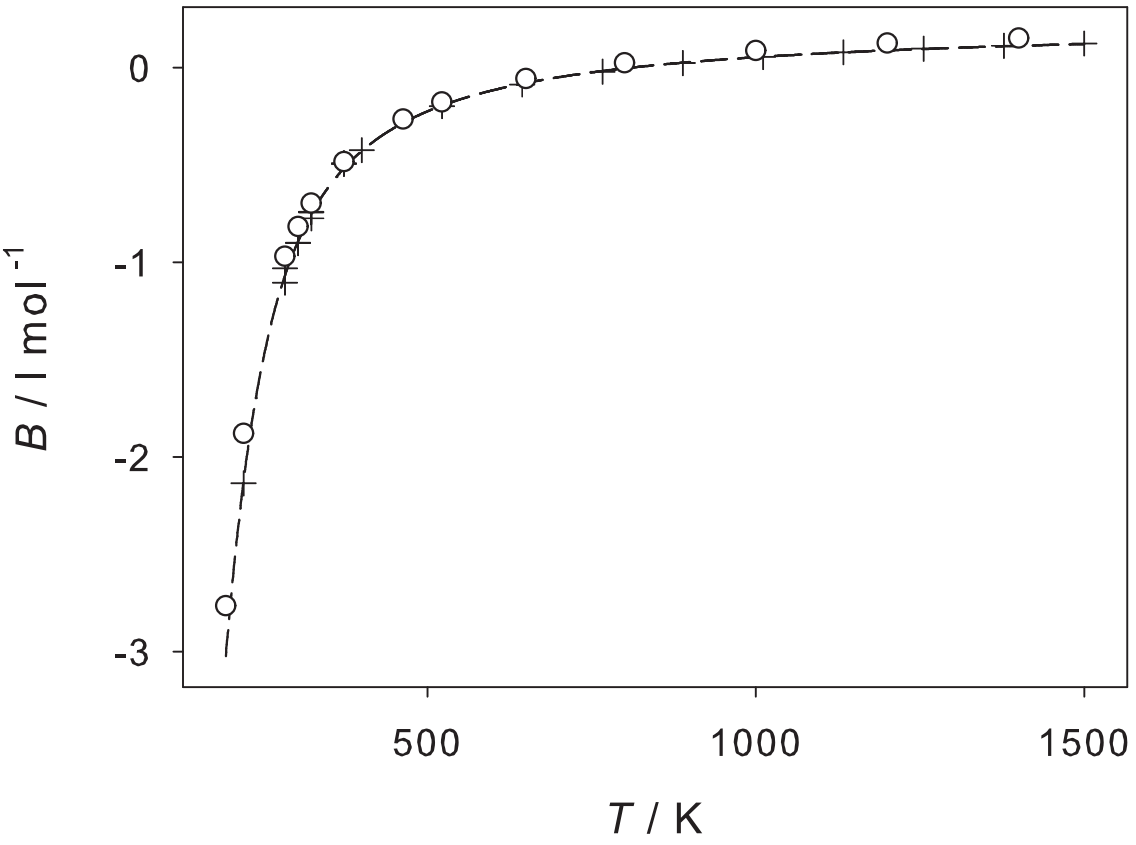

Fig. 7. Isothermal vapor-liquid phase diagrams of the binary system $C_2H_4 + C_4F_{10}$ at 268.13 K (△), 278.36 K (○), 288.16 K (□) and 298.13 K (◊): (full symbols) experimental data, this work, (empty symbols) simulation results, this work, — PR EOS, Wong-Sandler mixing rule, this work, ··· PR EOS, quadratic mixing rule, this work. The error bars of the data are not shown if they are within symbol size.

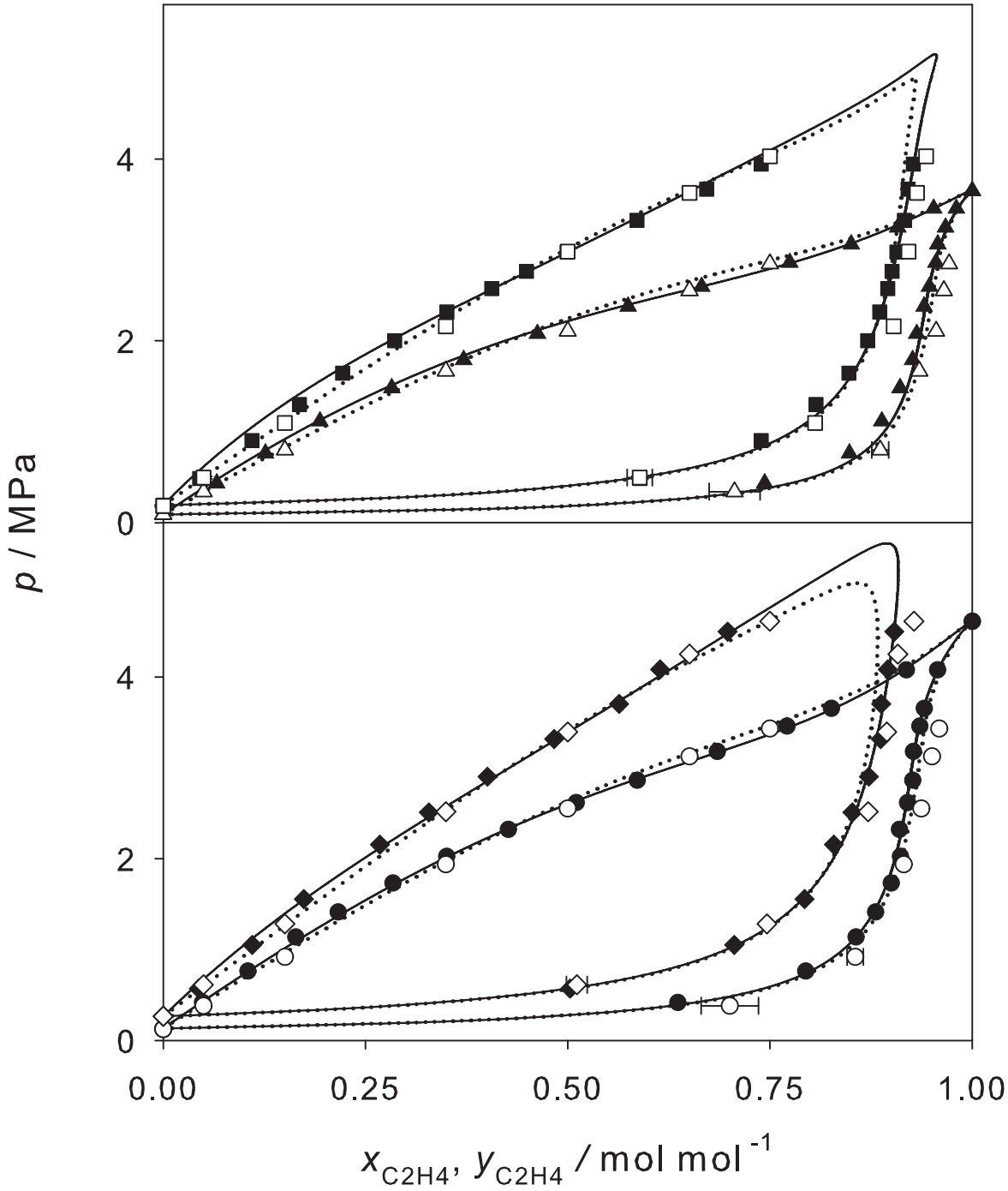

Fig. 8. NRTL model parameters $\tau_{C2H4,C4F10}$ (top), $\tau_{C4F10,C2H4}$ (center) and PR EOS binary interaction parameter $k_{C2H4,C4F10}$ (bottom) over the temperature: — model parameter correlations (cf. equations (12) - (15)), $(\cdots)$ critical temperature of C_2H_4.

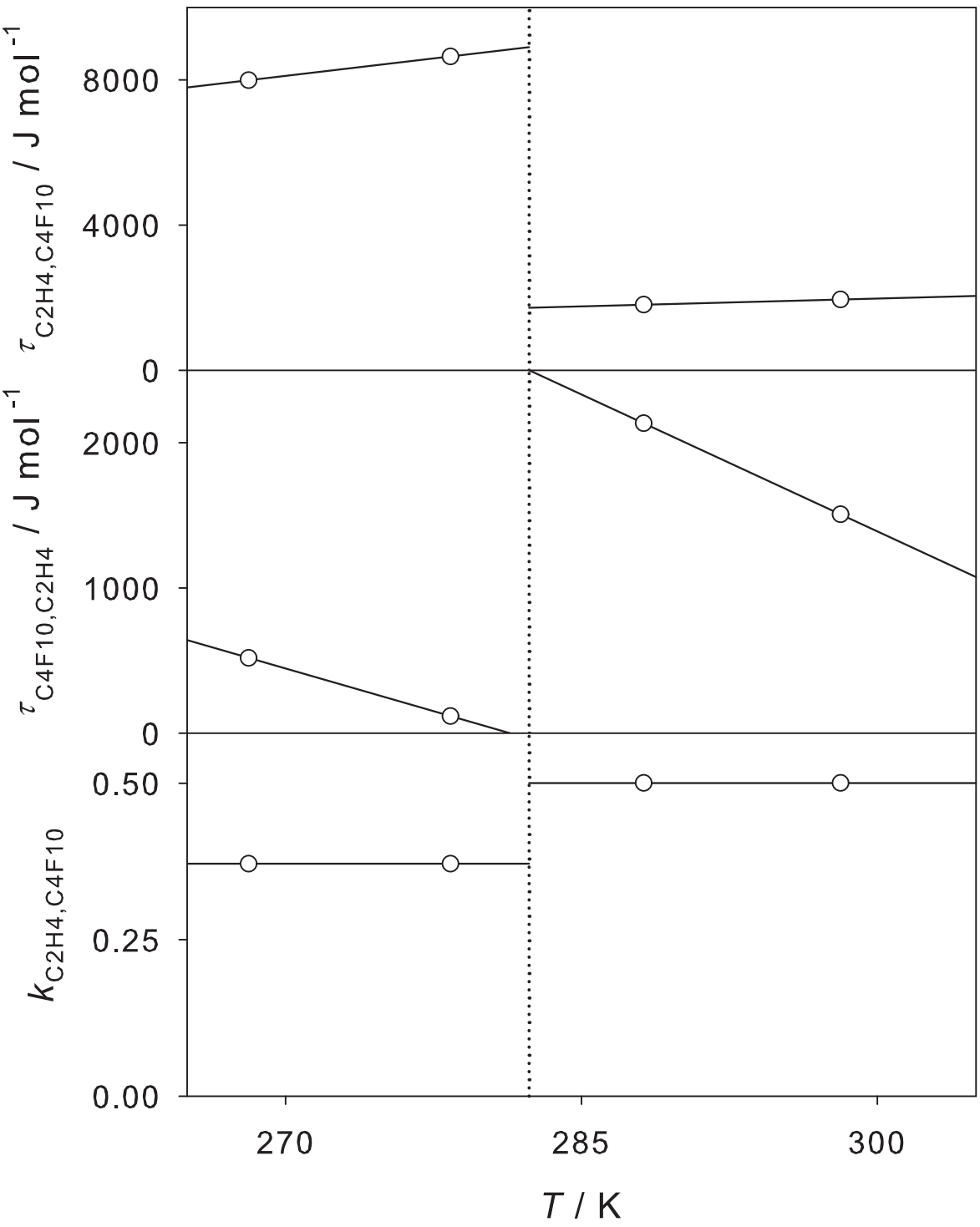

Fig. 9. Relative volatility $\alpha_{C2H4,C4F10}$ over mole fraction x_{C2H4} for C_2H_4 + C_4F_{10} at 268.13 K (△), 278.36 K (○), 288.16 K (□) and 298.13 K (◊): (full symbols) experimental data, this work, (empty symbols) simulation data, this work, — PR EOS, Wong-Sandler mixing rule, this work, ··· PR EOS, quadratic mixing rule, this work. The error bars of the data are not shown if they are within symbol size.